Effect of Iron Concentration on the Growth of Carbon Nanotubes on Clay Surface

Fu Huakang, Du Miao,* and Zheng Qiang

Key Laboratory of Macromolecule Synthesis and Functionalization, Ministry of Education, Department of Polymer Science and Engineering, Zhejiang University, Hanghzou, 310027, China

ABSTRACT: The successful growth of carbon nanotubes (CNTs) on montmorillonite (MMT) precursors treated with different concentrations of ferric nitrate at 50 °C (MMT(Fe)-50) and 100 °C (MMT(Fe)-100) was achieved via the in situ chemical vapor deposition (CVD) of acetylene. The as-obtained MMT-CNTs composites were characterized using X-ray diffraction, inductively coupled plasma emission spectrometry, scanning electron microscopy, and transmission electron microscopy. All Fe^{3+} ions were intercalated into the MMT interlayers at either 50 or 100 °C in the case of $[Fe^{3+}]/[clay] = 1$. However, the iron content in MMT(Fe)-100 increased rapidly with the amount of ferric nitrate added, whereas the iron content in MMT(Fe)-50 did not exhibit significant changes. On the other hand, the physical and chemical adsorption of Fe^{3+} onto the MMT surface was believed to be responsible for the great diversity of iron contents in MMT(Fe)-50 and MMT(Fe)-100 at the same $[Fe^{3+}]/[clay]$ ratios. Moreover, the CNT yield showed variation similar to the iron content because the CNTs yield depends primarily on the amount of catalyst available. The CNTs embedded onto MMT(Fe)-100 exhibited narrower diameter distributions than those on the MMT(Fe)-50 precursors, with more CNTs with diameters less than 50 nm on the former. It is suggested that a porous structure with many pores formed by iron species and MMT laminas is related to the morphology and structure of CNTs embedded on the surface of MMT.

KEYWORDS: montmorillonite, carbon nanotubes, in situ growth, interlayer, adsorption, iron concentration

1. INTRODUCTION

The richness and diversity of the properties (e.g., mechanical, electronic, thermal, and chemical) of carbon nanotubes (CNTs) have motivated extensive research on their synthesis, functionalization, and potential applications.[1-10] Carbon nanotubes can be synthesized by different techniques including carbon arc discharge,[11,12] laser ablation,[13] chemical vapor deposition (CVD),[14-16] and so on. Among these approaches, CVD has gained ground because of its convenience and cost-effectiveness, despite the fact that other techniques produce CNTs with higher yield and quality. Unlike other technologies, the utilization of CVD in conjunction with patterned catalyst arrays affords primarily unbundled CNTs because of their growth from specific surface sites.[17-19] The nature, yield and quality of CNTs produced by CVD are influenced by many technological parameters, such as temperature, the gas throughput, the carbon feeding gas, catalysts, time of deposition and so on. To date, numerous metallic catalysts derived from the reduction of transition metal salts have been employed into the process of CNTs growth, such as $FeCl_3$,[20] $Fe(NO_3)_3$, $FeSO_4$,[21] $Ni(NO_3)_2$[22] and Co/MgO mixed oxide powders.[1,2] These metallic catalysts are usually supported by various high surface area substrates, such as alumina,[23] silica,[24,25] mesoporous silica,[26] clays,[27-30] zeolites,[31] and so on. Montmorillonite (MMT), a kind of cationic clay, possesses unique swelling, intercalation, and ion-exchange properties that enable it to restructure into various valuable derivatives.[31] In situ growth of CNTs on MMT layers (MMT-CNTs composites) could provide another interesting class of materials for potential application in polymer reinforcement.[32] It is found that CNTs could be grown on clays and the as-obtained products could be directly filled into a nylon-6 matrix to significantly improve its tensile strength.[28]

MMT is the most common and ubiquitous clay mineral and it is made of one aluminum octahedral layer lying between two silicon tetrahedral layers. MMT has a negatively charged surface owing to the substitution of Al^{3+} ions in the octahedral layer by Mg^{2+} and Fe^{2+} ions, as well as of Si^{4+} ions in the tetrahedral layer by Al^{3+} ions. Usually, a single vacant site in every three octahedral positions exists. During high-temperature thermal treatment, the metal cations in interlayers of MMT have a chance to migrate from the inner pores to the empty octahedral sites, causing an increase in the octahedral layer occupancy.[29,33,34] When iron-containing clays are heated at around 700 °C, some ferric oxides from the extraction and agglomeration of structural iron atoms would be formed on the external surfaces of clays as evidenced by the bronzing color of the clay after thermal treatment without losing the lamellar structure of the clays. Moreover, such processes are important because the growth of CNTs through CVD occurs at around 700 °C using transition metal oxides such as Fe as catalyst.[7-9] Therefore, in situ CNTs generation is related directly to the
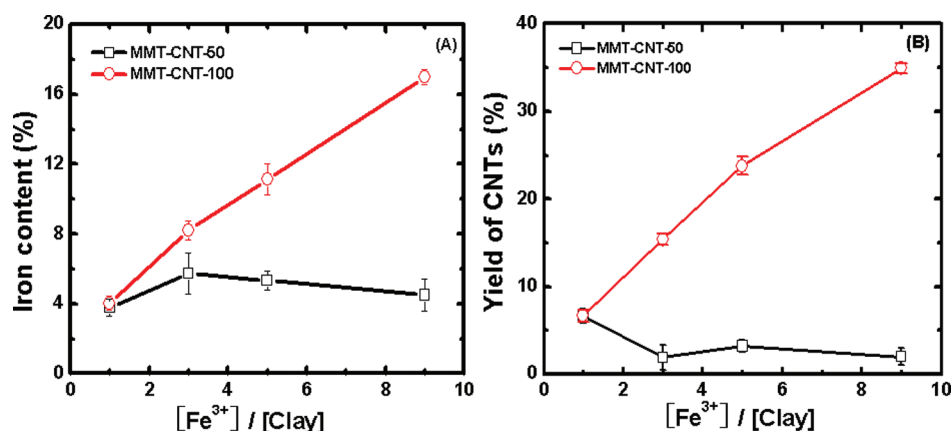
Figure 1. Effect of $[Fe^{3+}]$/[clay] ratio on (A) iron content and (B) yield of carbon in MMT(Fe)-50 and MMT(Fe)-100.
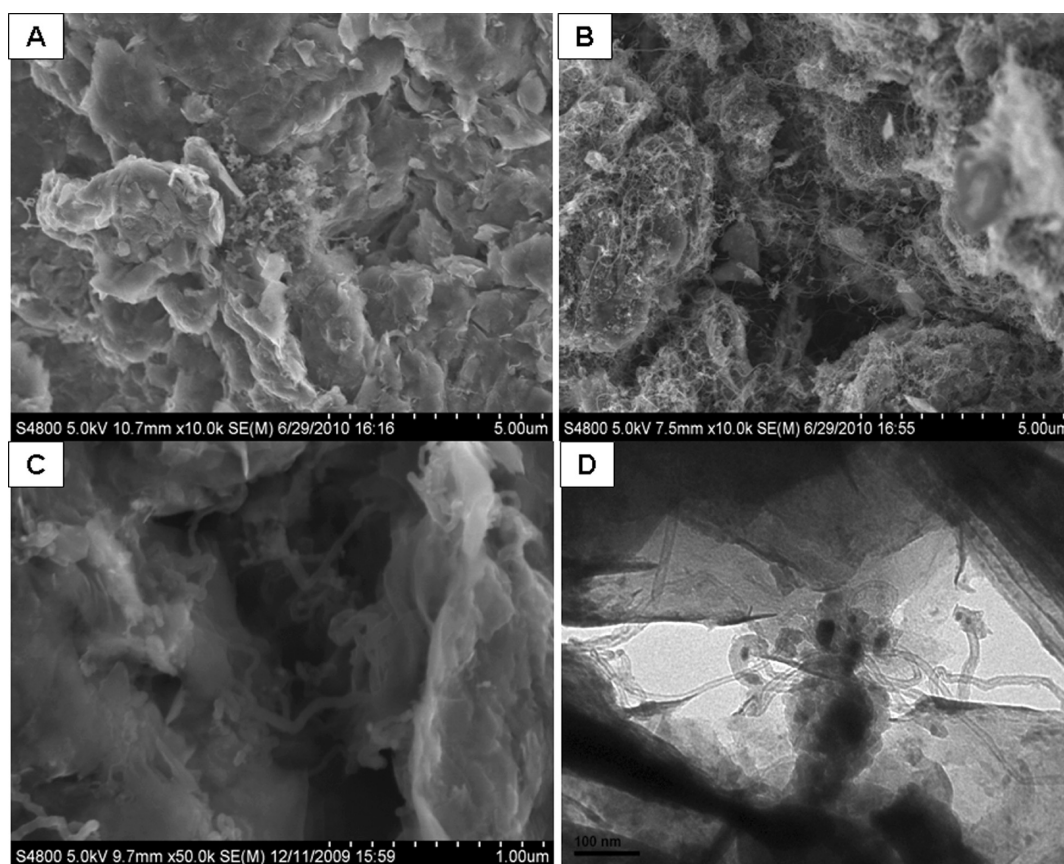

Figure 2. SEM images of CNTs grown on (A) MMT(Fe)-50(9), (B, C) MMT(Fe)-100(9). TEM images of CNTs grown on (D) MMT(Fe)-100(9).

presence and phases of iron species on the clay substrate, a finding that has not received much attention yet.

In the present work, we try to deposite catalyst precursors $(Fe(NO_3)_3)$ onto sodium-montmorillonite (Na^+MMT) by the ion-exchange reaction, and experimentally controlled the iron content in MMT with varying initial exchanged $Fe(NO_3)_3$ contents and reaction temperatures. MMTs treated with $Fe(NO_3)_3$ were initially subjected to calcination and then CVD treatment at around 700 °C to grow in situ CNTs. The as-obtained MMT-CNT composites were characterized by X-ray diffraction (XRD), scanning electron microscopy (SEM), and transmission electron microscopy (TEM). Interestingly, changes in the iron content of MMTs and ion-exchange

reaction temperature exhibited remarkable effects on the structure of the resulting MMT-CNTs composites.

2. MATERIALS AND METHODS

2.1. Materials and Synthetic procedure. The clay used in the current work, Na^+MMT (20 μm) containing 4.23 wt % sodium and 1.60 wt % iron, was obtained from Nanocor Co. Its cation-exchange capacity (CEC) is equal to 145 mequiv/100 g clay.

The catalyst precursor was the metal salt of $Fe(NO_3)_3 \cdot 9H_2O$, which was deposited onto the clay substrate through an ion-exchange reaction with the sodium ions of the parent clay by mixing a clay suspension with an aqueous solution of $Fe(NO_3)_3$. The amounts of $Fe(NO_3)_3$ used in the ion-exchange reactions were equivalent to 1, 3, 5, and 9 times the CEC of Na^+MMT. The $[Fe^{3+}]$/[clay] ratios ([clay]
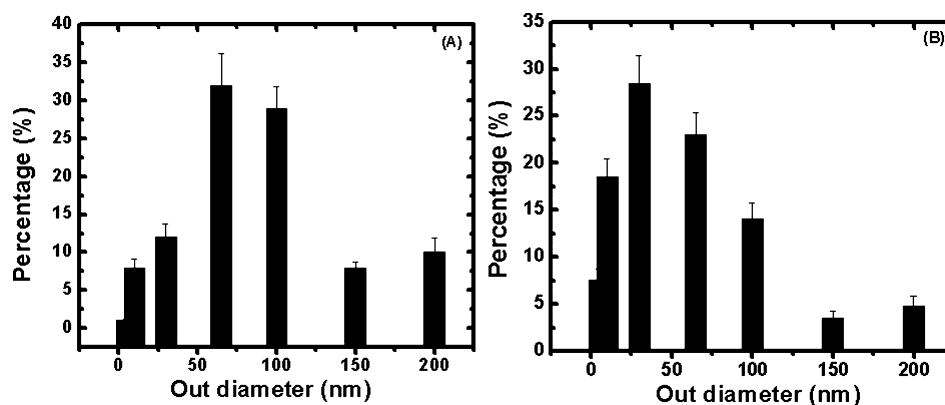
Figure 3. Diameter distributions of CNTs grown in situ on (A) MMT(Fe)-50(9) and (B) MMT(Fe)-100(9).

= 3[Na$^+$], the molar concentration of sodium can be calculated from CEC) were 1, 3, 5, and 9. The ion-exchange reactions with various [Fe^{3+}]/[clay] ratios were performed at 50 or 100 °C for 10 h with vigorous stirring to ensure complete exchange of the pristine sodium ions. Then, the mixture was centrifuged and washed with deionized water. The residue was dried overnight at 80 °C, ground, and then sieved using 200 meshes (with a diameter of 74 μm) to obtain particles. The particles were further calcined at 500 °C for 3 h to ensure that iron ions or complexes, which are discussed below, deposited on the clay surface were oxidized completely into ferric oxides.

The above precursors were placed in a horizontal fixed bed flow reactor for CVD treatment at 700 °C for 20 min, using a gas mixture of acetylene (C$_2$H$_2$) and Ar 1/6 (v/v) as carbon source. The as-obtained MMT precursors and the MMT-CNT composites were coded as MMT(Fe)-T(x) and MMT(Fe)-CNT-T(x), respectively (T = ion-exchange reaction temperature, x = [Fe^{3+}]/[clay] ratio). MMT(Fe)-T and MMT(Fe)-CNT-T represented a group of MMT-(Fe)-T(x) and MMT(Fe)-CNT-T(x), respectively. MMT(Fe)-T(x) after calcination was hereafter abbreviated as MMT(Fe)-T(x)-c.

2.2. Characterization. XRD patterns were obtained on a Rigaku D/max-III B X-ray diffractometer equipped with CuKα radiation (λ = 0.154 nm) using a generator voltage of 40 kV and a generator current of 300 mA, and a scan rate of 3°(2θ)/min was applied for the analysis. The morphologies of the samples were observed by TEM using a JEM-1230 system with a constant acceleration spectrometer and 50 mCi^{57} Co(R$_h$) source moving at room temperature and by SEM (Hitachi-S4800). The diameter distribution of CNTs was estimated by studying the diameter of around 100 individual CNTs in TEM images.

Iron contents of the as-prepared samples were measured using inductively coupled plasma (ICP) atomic emission spectrometry (ICP-AES) with a multichannel type detector (MKII, Jarrell-Ash Plasma Atom Com). Prior to measurement, samples were dissolved in hydrofluoric acid to remove the MMT framework. Iron contents were then determined. N$_2$ adsorption−desorption isotherms were measured at liquid nitrogen temperature by a gas sorption analyzer (Quantachrome, NOVA1000). Prior to measurement, samples were outgassed at 100 °C for at least 3 h. The specific surface area (SSA) was calculated using the Brunaue-Emmet-Teller (BET) equation and the average pore diameter was evaluated using the Barrett−Joyner−Halenda method. The pore size distribution curves were fitted using the nonlocal density functional theory method.

3. RESULTS

The iron contents in MMT(Fe)-50 and MMT(Fe)-100 with various [Fe^{3+}]/[clay] ratios are shown in Figure 1A. The iron content in MMT(Fe)-50 does not exhibit significant change, whereas the iron content in MMT(Fe)-100 increases rapidly with increasing [Fe^{3+}]/[clay] ratio. The iron contents in both MMT(Fe)-50 and MMT(Fe)-100 are almost the same in the case of [Fe^{3+}]/[clay] = 1; however, the iron contents of

MMT(Fe)-100 at [Fe^{3+}]/[clay]>1 are much higher than that of MMT(Fe)-50. After calcination at 500 °C, the MMT(Fe)-50 and MMT(Fe)-100 act as precursors for the in situ deposition of carbon. Ignoring the amorphous carbon formed during the course of CVD, the yield of CNTs in terms of the ultimate mass loss in thermogravimetric measurement[35] increases (Figure 1B). With increasing [Fe^{3+}]/[clay] ratio, the yields of CNTs for MMT(Fe)-50 do not change dramatically, whereas those for MMT(Fe)-100 increase monotonously. In the case of [Fe^{3+}]/[clay] = 1, the CNTs yield is 6.6 wt % for both MMT(Fe)-50 and MMT(Fe)-100. However, at [Fe^{3+}]/[clay] = 9, the CNTs yield is only 2 wt % for MMT(Fe)-50 and 34.9 wt % for MMT(Fe)-100. Considering that the CNTs yield depends primarily on the catalyst content,[36] the consistency between panels A and B in Figure 1 is easier to understand.

Morphologies of the as-obtained products, MMT(Fe)-CNT-50(9) and MMT(Fe)-CNT-100(9), were examined by SEM and TEM. In Figure 2A, MMT(Fe)-CNT-50(9) is shown to have a small quantity of CNTs with tips attached to iron moieties appearing on the external layers of MMT. In contrast, the surface of MMT(Fe)-100(9) is covered by a mass of CNTs (Figure 2B). This phenomenon is consistent with the results from Figure 1B. Notably, in MMT(Fe)-CNT-100(9), some CNTs are embedded in the space between some clay laminas, each of which consists of several or even more single mineral layers, as indicated in Figures 2C and 2D. The hollow nature of the carbon tubes produced is evident in all systems. The outer diameter distribution of CNTs given in Figure 3 was estimated by counting the diameter of around 100 individual CNTs in the TEM images. A wide diameter distribution of CNTs for the two kinds of composites is observed. The outer diameter of the CNTs for MMT(Fe)-CNT-50(9) and MMT(Fe)-CNT-100(9) is between (5 and 200) nm, and their lengths reach up to a few micrometers. Interestingly, MMT(Fe)-CNT-100(9) possesses more CNTs with diameters smaller than 50 nm and a relatively homogeneous diameter distribution compared with MMT(Fe)-CNT-50(9). CNTs on MMT surfaces gained from the two precursors, MMT(Fe)-50 or MMT(Fe)-100, are believed to differ only slightly in quality because of the use of the same catalyst, substrate, gas source, and growth process of CNTs.

As previously mentioned, three abnormal phenomena are presented. (1) In the case of [Fe^{3+}]/[clay] = 1, the iron contents and the corresponding CNTs yields for both MMT(Fe)-50 and MMT(Fe)-100 precursors are the same. Nevertheless, at [Fe^{3+}]/[clay]>1, the iron contents and the CNTs yields for MMT(Fe)-100 precursors are much higher than those of MMT(Fe)-50. (2) The iron contents and CNTs
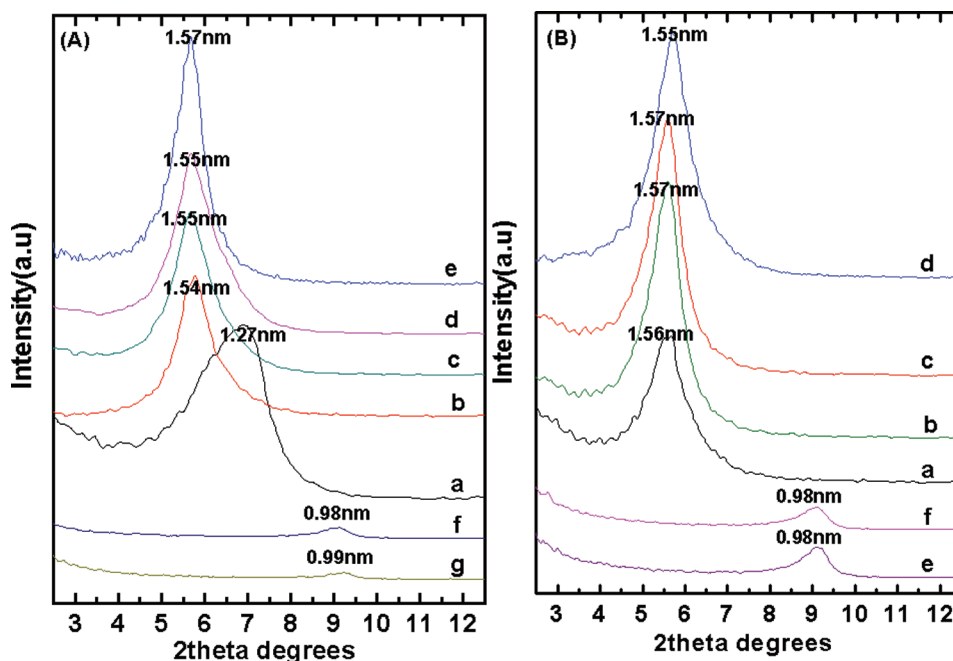
Figure 4. (A) XRD patterns from (a) initial Na⁺MMT, (b) MMT(Fe)-50(1), (c) MMT(Fe)-50(3), (d) MMT(Fe)-50(5), (e) MMT(Fe)-50(9), (f) MMT(Fe)-50(9)-*c*, (g) MMT(Fe)-CNT-50(9). (B) XRD patterns from (a) MMT(Fe)-100(1), (b) MMT(Fe)-100(3), (c) MMT(Fe)-100(5), (d) MMT(Fe)-100(9), (e) MMT(Fe)-100(9)-*c*, (f) MMT(Fe)-CNT-100(9).

yields for MMT(Fe)-50 precursors do not exhibit significant change, whereas those for MMT(Fe)-100 increase rapidly with the $[Fe^{3+}]/[clay]$ ratio. (3) The MMT(Fe)-CNT-100(9) composites possess larger amounts of CNTs with diameters smaller than 50 nm than MMT(Fe)-CNT-50(9). Moreover, most CNTs are generated on the external layer of MMT(Fe)-CNT-50(9). In MMT(Fe)-CNT-100(9), some CNTs are embedded in the space between MMT laminas. Aside from the $[Fe^{3+}]/[clay]$ ratio, the only difference between MMT(Fe)-50 and MMT(Fe)-100 is the ion-exchange reaction temperature. These three abnormal phenomena will be discussed below.

4. DISCUSSIONS

1. At $[Fe^{3+}]/[clay]$ = 1. $[Fe^{3+}]/[clay]$ = 1 suggests that the exchange reaction between Fe^{3+} and Na^+ ions is equivalent, that is, Na^+ ions within the interlayer space of MMT can be exchanged completely by Fe^{3+} ions,[37] and that all of the Fe^{3+} ions should impregnate into the interlayers of MMT. Metal ions always exist in the form of the hydrated metal ions in solution; however, for convenience, Fe^{3+} ions and Na^+ ions are used directly in the current study. Generally, the exchange process between Na^+ and Fe^{3+} ions can be easily achieved within several hours under room temperature,[38] suggesting that the reaction temperature has little effect on the ion-exchange process, as long as given enough reaction time. Thus in the present study, the exchange reaction continues for around 10 h, which is considered sufficient for the exchange between Na^+ and Fe^{3+} ions to occur no matter at 50 or 100 °C. Accordingly, in the case of $[Fe^{3+}]/[clay]$ = 1, all of the Fe^{3+} ions impregnated into the MMT interlayers and exchanged completely with the Na^+ ions. No excess Fe^{3+} for deposition on the external surface of the MMT at either 50 or 100 °C is obtained. The ion-exchange reaction between Na^+ and Fe^{3+} ions causes the d_{001} basal spacing of pristine MMT shift to a larger value (Figure 4). That is, the d_{001} basal spacing moves

from 1.27 nm for pristine Na⁺MMT to almost the same values of 1.54 nm for MMT(Fe)-50(1) and 1.56 nm for MMT(Fe)-100(1) after exchanging, are consistent with previous reports.[1,22] Consequently, the complete exchange reaction between Na^+ and Fe^{3+} ions is believed to be responsible for the same iron contents and the corresponding CNT yields for both MMT(Fe)-50(1) and MMT(Fe)-100(1) precursors.

2. At $[Fe^{3+}]/[clay]$>1. When $[Fe^{3+}]/[clay]$>1, the Fe^{3+} ions involved in the exchange reaction with Na^+ ions are in excess. The d_{001} basal spacing of both MMT(Fe)-50 and MMT(Fe)-100 at $[Fe^{3+}]/[clay]$>1 is (1.56 ± 0.02) nm (Figure 4). The value is very close to the value for $[Fe^{3+}]/[clay]$ = 1, indicating that the excess Fe^{3+} ions cannot further expand the interspace between MMT layers. During the exchange reaction, Fe^{3+} ions prefer to exchange with Na^+ ions first.[37,38] Once the exchanged Fe^{3+} ions in the interlayers of MMT are saturated, the excess Fe^{3+} ions will deposit on the external surface of the MMT layers in the form of Fe^{3+} ions or iron complexes. The difference in ion-exchange reaction temperatures that causes a remarkable discrepancy in the deposition of Fe^{3+} ions or iron complexes at the same $[Fe^{3+}]/[clay]$ ratio could be explained by the deposition of metal ions through physical and chemical adsorption.

Physical adsorption comes from intermolecular attractions between the adsorbent and adsorbate, which is reversible and appears to be in dynamic equilibrium at a certain temperature and concentration. The strong physical adsorption of the clay is derived from its high surface energy and is closely proportional to its SSA.[38] Figure 5 shows the effect of $[Fe^{3+}]/[clay]$ ratio on the SSAs of both MMT(Fe)-50 and MMT(Fe)-100 precursors. Trends similar to that in Figure 1 are observed, which points to two possible explanations:

(a) At 50 °C, the SSAs do not change with increasing $[Fe^{3+}]/[clay]$ ratio. During the ion-exchange reaction, the high instantaneous vapor pressure generated can open a few gaps between the MMT laminas and divide large laminas into
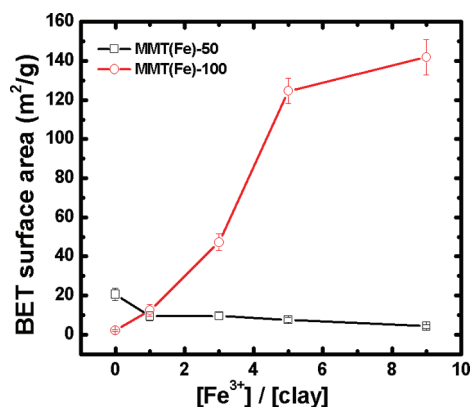
Figure 5. Effect of $[Fe^{3+}]/[clay]$ ratio on specific surface area of MMT(Fe)-50 and MMT(Fe)-100.

smaller ones, however, not strong enough to prop each single MMT layer apart.[39] In Figure 4, MMT(Fe)-50 and MMT(Fe)-100 are shown to possess the same d_{001} basal spacing. Low ion-exchange reaction temperatures (such as 50 °C) are not believed to generate high vapor pressure and enough energy to force the large MMT laminas apart and enlarge the SSA of MMT(Fe)-50. Therefore, more Fe^{3+} ions ($[Fe^{3+}]/[clay]>1$) could not intercalate into the MMT laminas and segregate them from each other. On the other hand, the Fe^{3+} ions are deposited to form large aggregations on the MMT external surface. The SSA in this case is small and only a limited amount of the excess Fe^{3+} ions could be accommodated, which is considered to be responsible for the low iron contents in

MMT(Fe)-50. Figure 6A shows a TEM image of the large aggregations deposited on the MMT(Fe)-50(9) surface and MMT layers stacked tightly, which agrees with the discussion above.

At 100 °C, the SSAs increase remarkably with increasing $[Fe^{3+}]/[clay]$ ratio. As illuminated above, high instantaneous vapor pressures are generated because of the gasification of boiling water throughout the reflux reaction at 100 °C, which is in favor of opening many gaps among MMT laminas and enlarging the SSA. Therefore, Fe^{3+} ions could easily insert into these gaps and then deposit in the form of small particles at 100 °C, as shown in Figure 6B and the inset. By increasing the amount of ferric nitrate, more Fe^{3+} ions are able to intercalate into the space between the MMT laminas, leading to further increases in the SSA for MMT(Fe)-100 with the $[Fe^{3+}]/[clay]$ ratio. Therefore, the enlarged MMT surface could accommodate more Fe^{3+} ions, thus explaining the high iron content in MMT(Fe)-100. The space structure of the laminas will be discussed further in Morphologies Section. The SSA of pristine Na^+MMT from Table 1 is only 8.24 cm^2/g because of serious aggregation; however, after the ion-exchange reaction with ferric nitrate at 100 °C, the SSA increases greatly, and the maximum SSA, 141.83 cm^2/g, is achieved in MMT(Fe)-100(9). Brownian motion is more intense at 100 °C than at 50 °C, which is not favorable to desorption of the Fe^{3+} ions. However, the competition between Brownian motion and the increase in SSA resulted in the adsorption of Fe^{3+} ions at 100 °C.

Another factor contributing to the great diversity of iron contents in MMT under different temperatures is chemical adsorption, which originates from the chemical bonding
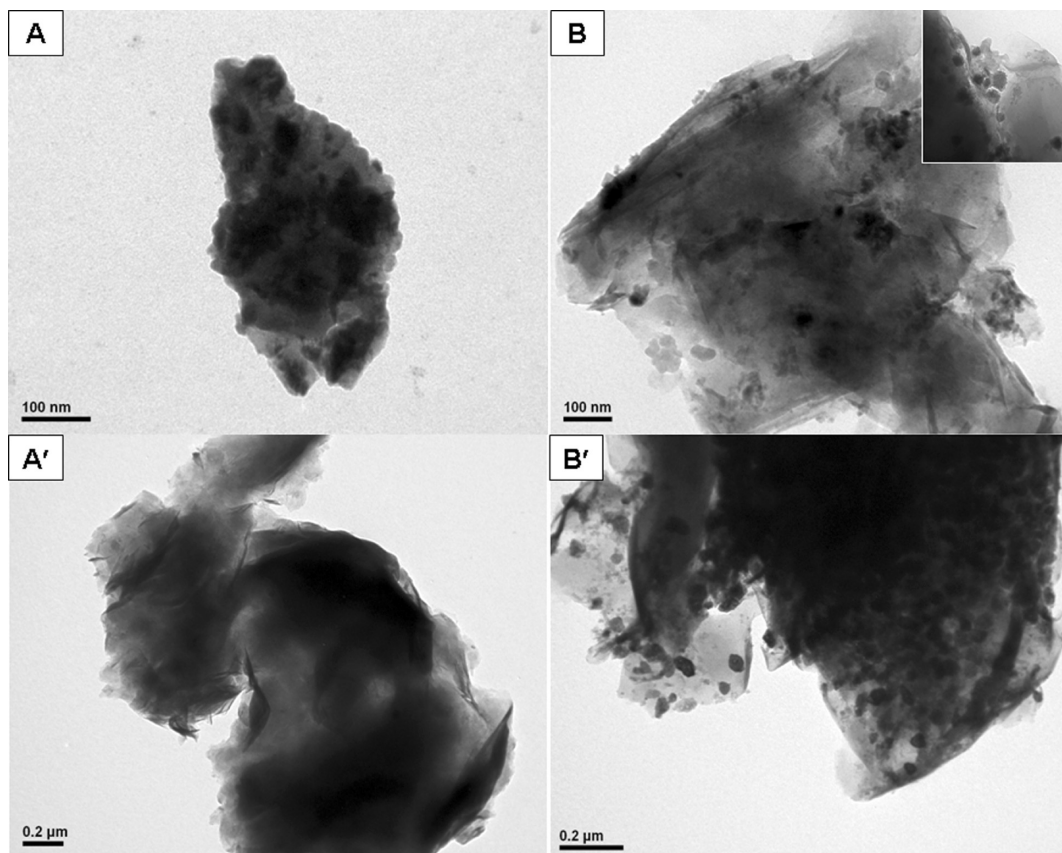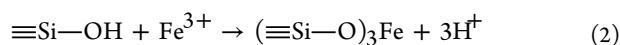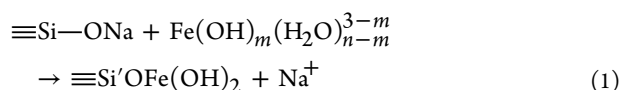

Figure 6. TEM images of (A) MMT(Fe)-50(9), (B) MMT(Fe)-100(9), (A′) MMT(Fe)-50(9)-*c*, and (B′) MMT(Fe)-100(9)-*c*.

Table 1. Textural Properties of the Pristine and Ferric-Nitrate-Treated MMT

sample	iron contents (wt %)	special surface area (SSA) (cm²/g)	average pore diameter (nm)	pore volume (cm³/g)
Na⁺MMT	1.3	8.24 ± 1.77	11.6	0.081
MMT(Fe)-50(0)	0	20.52 ± 3.1	9.7	0.081
MMT(Fe)-50(1)	3.78 ± 0.49	9.41 ± 1.9	12.2	0.036
MMT(Fe)-50(3)	5.73 ± 1.16	9.49 ± 1.56	11.2	0.031
MMT(Fe)-50(5)	5.34 ± 0.54	7.57 ± 1.21	14.8	0.020
MMT(Fe)-50(9)	4.51 ± 0.90	4.17 ± 1.74	16.5	0.018
MMT(Fe)-100(0)	0	2.18 ± 0.43	13.8	0.016
MMT(Fe)-100(1)	4.03 ± 0.41	16.35 ± 2.99	9.5	0.052
MMT(Fe)-100(3)	8.21 ± 0.53	47.21 ± 4.37	7.9	0.113
MMT(Fe)-100(5)	11.13 ± 0.90	124.54 ± 6.45	6.9	0.195
MMT(Fe)-100(9)	16.99 ± 0.42	141.83 ± 9.1	6.1	0.198
MMT(Fe)-50(1)-c	3.53 ± 1.12	61.57 ± 4.17	10.3	0.101
MMT(Fe)-50(9)-c	4.27 ± 0.87	49.71 ± 4.76	12.3	0.062
MMT(Fe)-100(1)-c	4.29 ± 1.29	112.32 ± 7.23	7.7	0.119
MMT(Fe)-100(9)-c	16.73 ± 2.94	156.85 ± 8.21	10.6	0.220

between the adsorbent and absorbate. In the present study, chemical adsorption is related to the surface complexation reaction between the iron hydrolysate and MMT surface. Considering that the edges of the clays are the effective surfaces of a mixture of oxide-gibbsite and silica, some metal ions would be adsorbed as pure oxide phases on the surface of MMT or the space between MMT laminas.[40] Bhattacharyya et al.[41] pointed out that clay—Fe^{3+} adsorption complex is more stable than the isolated clay or Fe^{3+} ions in aqueous medium, and the formation of moderately strong bonding between Fe^{3+} ions and clay edges leads to the decrease in the overall energy of the system. Fe^{3+} ions usually exist in two forms in water: one is the hydrated Fe^{3+} ion, the other is the hydrolysate of Fe^{3+} ions. In the present system, the active functional groups ($\equiv Si-ONa$ and $\equiv Si-OH$) on the Na⁺MMT surface have the potential to react with the hydrolysate of Fe^{3+} ions and hydrated Fe^{3+} ions to form surface complexes as shown in the following

$$\equiv Si-ONa + Fe(OH)_m(H_2O)_{n-m}^{3-m}$$
$$\rightarrow \equiv Si'OFe(OH)_2 + Na^+ \quad (1)$$

$$\equiv Si-OH + Fe^{3+} \rightarrow (\equiv Si-O)_3Fe + 3H^+ \quad (2)$$

where $Fe(OH)_m(H_2O)_{n-m}^{3-m}$ is the hydrolysate of Fe^{3+} ions in aqueous solution.

$$Fe^{3+} + nH_2O \rightarrow Fe(OH)_m(H_2O)_{n-m}^{3-m} + mH^+ (n > m) \quad (3)$$
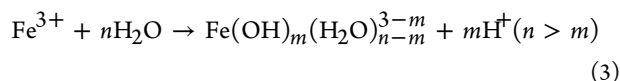
High temperature favors the hydrolysis reaction of Fe^{3+} ions because of their endothermic characteristic,[40] which generates more hydrolysates and complexes between the surface active

functional groups on the MMT surface. On the other hand, high temperature also favors the formation of complexes between the surface active functional groups of MMT and hydrated Fe^{3+} ions, because the loss of bound water is easy at high temperature, which is necessary during the process of chemical adsorption for hydrated Fe^{3+} ions onto the clay surface. Wang et al.[40] showed that adsorption of Ni^{2+} ions from aqueous solution on clay surface increases with increasing temperature, which is attributed to the higher hydration degree of Ni^{2+} ions at high temperature.

More hydrogen ions are released during both the hydrolysis reaction of Fe^{3+} ions and the chemical adsorption between $\equiv Si-OH$ and hydrated Fe^{3+} ions from eqs 2 and 3. This would lead to decreases in the pH of the system. As mentioned above, high temperature favors eqs 2 and 3. Thus, high ion-exchange reaction temperatures (100 °C) lead to lower pH values than low reaction temperature (50 °C). To confirm this hypotheses, the change in pH with the reaction time during the hydrolysis of $Fe(NO_3)_3$ in deionized water at 50 and 100 °C was determined (Figure 7). The pH of the $Fe(NO_3)_3$ aqueous
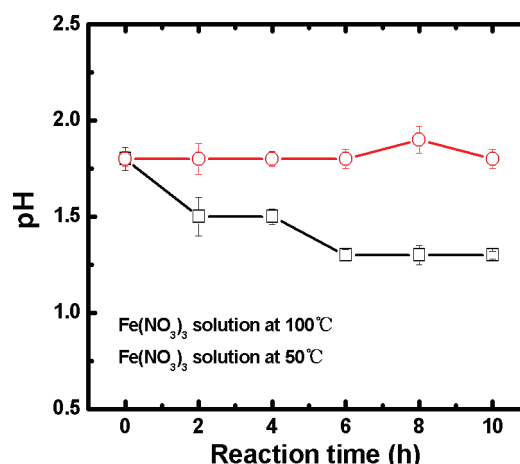

Figure 7. Dependence of pH value for $Fe(NO_3)_3$ aqueous solution on reaction time under different temperatures.

solution is maintained at a constant value at 50 °C but decreased at 100 °C, thus agreeing with the previous inference.

The complexes precipitate out at pH 2−4, changing the color of the MMT surface to bronze. Thus, the change in color could provide a simple and rough criterion for the hydrolysis degree of Fe^{3+} ions. Figure 8 shows that the color of pristine Na⁺MMT is khaki, whereas MMT(Fe)-50 with different $[Fe^{3+}]/[clay]$ ratios and MMT(Fe)-100(1) appear to be sandy beige; the color is attributed to low iron contents or even absence of hydrolysis reaction of Fe^{3+} ions in aqueous solution. Few of the complexes are precipitated out. MMT(Fe)-100(3), MMT(Fe)-100(5), and MMT(Fe)-100(9) are bronze-colored, which is attributed to the high contents of iron complexes generated on the MMT surface at 100 °C.

In summary, high temperature is favorable for the physical and chemical adsorption of Fe^{3+} ions onto MMT surfaces.

3. Morphologies. In the pristine Na⁺MMT suspension aqueous solution, MMT layers can form many various aggregate structures, such as face—top aggregation, face—face aggregation, and top—top aggregation, because of the diversity of surface charge over clay layers and the irregularity of the clay particles.[42] In most cases, the face-top aggregation of MMT layers will form a disordered porous structure called "house of
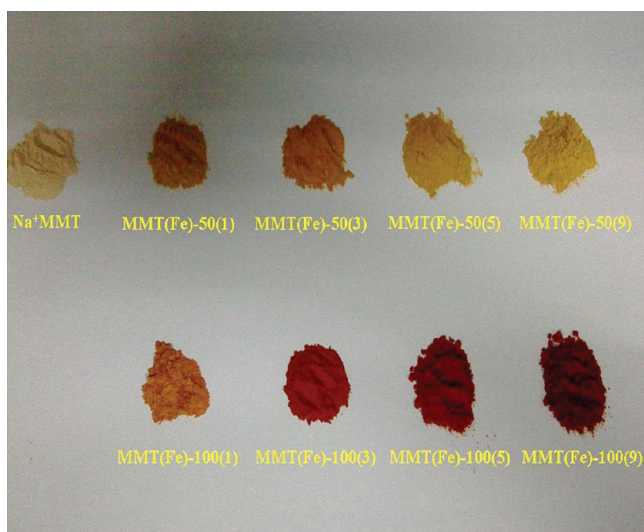
Figure 8. Color of pristine Na⁺MMT, MMT(Fe)-50, and MMT(Fe)-100.

cards".[43] Adding Fe^{3+} ions to the clay suspension causes the decrease of the electrical potential on the clay surface and gives rise to the development of face−face aggregation, which favors the formation of slit-shaped pores.[38,43] As mentioned above, a mass of Fe^{3+} ions and iron complexes are deposited on MMT external surface or in the space between the laminas at 100 °C rather than 50 °C after ion-exchange. Accordingly, many micropores would be generated because of the deposition of these iron species in the MMT slit-shaped pores. Further assembly of these iron species could shape many new micopores, as schematically represented in Figure 9. The
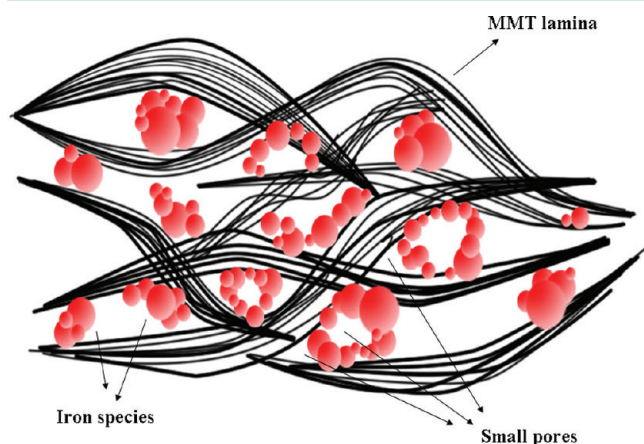

Figure 9. Schematic diagram of the porous structure of ferric nitrate treated MMT at 100 °C.

pore diameter distributions of pristine Na⁺MMT, MMT(Fe)-50, and MMT(Fe)-100 with various $[Fe^{3+}]/[clay]$ ratios were measured and shown in Figure 10. All the samples exhibit a wide pore size distribution from 5 to 100 nm. The number of small-sized pores (5 to 30 nm) in MMT(Fe)-50 samples is slightly reduced with increasing $[Fe^{3+}]/[clay]$ ratio (Figure 10A), suggesting that the assembled shape of the MMT layers probably changed from face-top aggregation to face−face aggregation to some degree after soaking in $Fe(NO_3)_3$ aqueous solution for a long time, which is supported by the total pore volume reduction from 0.036 cm^{-3}/g for MMT(Fe)-50(1) to

0.018 cm^{-3}/g for MMT(Fe)-50(9) (Table 1). Nevertheless, the number of small-sized pores increases with $[Fe^{3+}]/[clay]$ ratio for MMT(Fe)-100, supported by the increase of pore volume from 0.052 cm^{-3}/g for MMT(Fe)-100(1) to 0.198 cm^{-3}/g for MMT(Fe)-100(9), as shown in Table 1. Correspondingly, the average pore diameter is reduced from 9.5 nm for MMT(Fe)-100(1) to 4.1 nm for MMT(Fe)-100(9). The iron contents of pristine Na⁺MMT, MMT(Fe)-50, and MMT(Fe)-100, and the corresponding porous structure parameters are summarized in Table 1. Iron contents of MMT(Fe)-50(1), MMT(Fe)-50(9), MMT(Fe)-100(1), and MMT(Fe)-100(9) did not exhibit significant change even after calcination at 500 °C, suggesting that iron species consisting of hydrated Fe^{3+} ions and the iron complexes became ferric oxides during high-temperature thermal treatment. The escape of interlayer water molecules results in substitution of the original interlayer space by many micopores;[44] therefore, the average pore diameters of MMT-(Fe)-50(1), MMT(Fe)-50(9), and MMT(Fe)-100(1) undergoing high-temperature thermal treatment are reduced, as listed in Table 1. The escape of water molecules around the hydrated Fe^{3+} ions and iron complexes during thermal treatment perforates some small-sized pores (5 to 10 nm) to form larger pores (10 to 30 nm), as shown in Figure 10B.

In the current study, only part of the hydrated Fe^{3+} ions in MMT could lose water molecules after calcination and migrate to the external surface of the MMT after high-temperature thermal treatment.[35] The rest are restricted in the interlayer and become incapable of CNTs growth. Therefore, most CNTs grow in situ on the MMT external surface both for MMT(Fe)-CNT-50 and MMT(Fe)-CNT-100 (Figure 2A, B). However, because the special structure formed in MMT(Fe)-100 precursors (Figure 9) was substantially reserved after calcination, some CNTs embedded in the space between the MMT laminas were found as shown in Figures 2C and 2D. Considering the irreversibility of water molecules escaping during high-temperature thermal treatment, the d-spacing both for MMT(Fe)-50(9) and MMT(Fe)-100(9) decreases from 1.5 to 0.96 nm, as shown in Figure 4.

The size and dispersion of the iron species on MMT surface do not exhibit significant change after calcination, as shown in panels A′ and B in Figure 6′. The diameter of CNTs generated by CVD in the current study depends on the size of ferric oxides formed on the MMT surface,[36] which is almost similar to the size of the iron species before high-temperature thermal treatment. Because of the strong impact effect of the high instantaneous vapor pressure at 100 °C, the size of the deposited iron species in MMT(Fe)-100 is smaller than that in MMT(Fe)-50, which is responsible for the fact that MMT(Fe)-CNT-100 possess more CNTs with diameters smaller than 50 nm than does in MMT(Fe)-CNT-50.

5. CONCLUSIONS

Increasing the $[Fe^{3+}]/[clay]$ ratio does not always lead to increase in as-obtained iron contents in MMT by ion-exchange, rather, the increase appears to depend on the reaction temperature. In the case of low ion-exchange temperature, weak physical and chemical adsorption between iron ions and MMT surface causes the iron content in MMT to become almost independent of the initial $[Fe^{3+}]/[clay]$ ratio. The iron ions are primarily deposited on the external surface of the MMT, which is in favor of the deposition of iron ions with large sizes attributed to the unrestricted border. Moreover, more CNTs with large diameters can be grown in situ and embedded
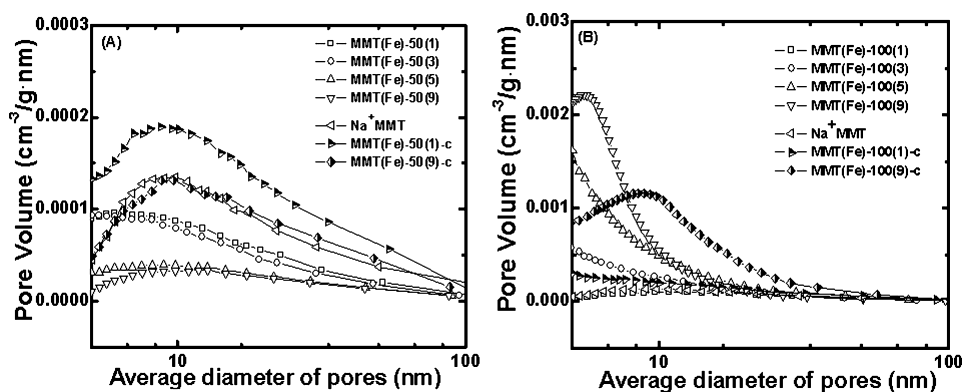
Figure 10. Pore diameter distribution curves from (A) initial Na+MMT, MMT(Fe)-50(1)-*c*, MMT(Fe)-50(9)-*c*, and MMT(Fe)-50; (B) MMT(Fe)-100(1)-*c*, MMT(Fe)-100(9)-*c*, and MMT(Fe)-100.

on the external surface of the MMT. At 100 °C, the high instantaneous vapor pressure generated by the gasification process of boiling water tends to open many gaps between the MMT laminas, thereby enlarging the SSA of MMT to some extent and resulting in the relatively strong physical and chemical adsorption of iron onto MMT surface. Adsorption then becomes stronger with increasing $[Fe^{3+}]/[clay]$ ratio. Owing to the restriction of the MMT laminas, more iron ion deposits with small size are formed and more CNTs with small diameters grown in situ are embedded in the space between some MMT laminas. It is proposed that only when $[Fe^{3+}]/[clay] = 1$, does the as-obtained iron content in MMT, as well as the CNTs content, become independent of the ion-exchange reaction temperature.

■ AUTHOR INFORMATION

Corresponding Author
*E-mail: dumiao@zju.edu.cn.

Notes
The authors declare no competing financial interest.

■ ACKNOWLEDGMENTS

■ REFERENCES

(1) Bakandritsos, A.; Simopoulos, A.; Petridis, D. *Chem. Mater.* **2005**, *17*, 3468−3474.
(2) Coquay, P.; Peigney, A.; Vandenberghe, R. E.; Laurent, C. *J. Phys. Chem. B* **2002**, *106*, 13199−13203.
(3) Ajayan, P. M. *Chem. Rev.* **1999**, *7*, 1787−1799.
(4) Takaba, H.; Katagiri, M.; Kubo, M.; Vetrivel, R.; Miyamoto, A. *Microporous Mesoporous Mater.* **1999**, *3*, 449−454.
(5) Dresselhaus, M. S.; Dresselhaus, G.; Eklund, P. C. *Science of Fullerenes and Carbon Nanotubes*; Academic Press: New York, 1996.
(6) Tanaka, K.; Okahara, K.; Okada, M.; Yamabe, T. *Fullerene Sci. Technol.* **1993**, *1*, 137−142.
(7) Miyagawa, H.; Drzal, L. T. *Polymer* **2004**, *45*, 5163−5170.
(8) Beyer, G. *Fire Mater.* **2002**, *26*, 291−293.
(9) Frackowiak, E.; Béguin, F. *Carbon* **2002**, *40*, 1775−1787.
(10) Yogeeswaran, G.; Cheng, P.; Yang, L.; Phillip, E. L.; Padraig, M.; Enrique, B.; James, M. T.; Roberto, B. *ACS Appl. Mater. Interfaces* **2011**, *3*, 129−134.
(11) Iijma, S. *Nature* **1991**, *354*, 56−58.
(12) Journet, C.; Maser, W. K.; Bernier, P.; Loiseau, A.; Lefrant, S.; Lee, R.; Fischer, J. E. *Nature* **1997**, *388*, 756−758.

(13) Fischer, J. E.; Rao, A. M.; Eklund, P. C.; Smalley, R. E. *Appl. Phys. A: Mater. Sci. Process.* **1998**, *67*, 29−34.
(14) Huang, Z. P.; Xu, J. W.; Ren, Z. F.; Wang, H. J.; Siegal, M. P.; Provencio, P. N. *Appl. Phys. Lett.* **1998**, *73*, 3845−3847.
(15) Ren, Z. F.; Huang, Z. P.; Xu, J. W.; Wang, H. J.; Bush, P.; Siegal, M. P.; Provencio, P. N. *Science* **1998**, *282*, 1105−1107.
(16) Nikolaev, P.; Bronikowski, M. J.; Bradley, R. K.; Fohmund, F.; Colbert, D. T.; Smith, K. A.; Smalley, R. E. *Chem. Phys. Lett.* **1999**, *313*, 91−97.
(17) Hou, H.; Schaper, A. K.; Jun, Z.; Weller, F.; Greiner, A. *Chem. Mater.* **2003**, *15*, 580−585.
(18) Hongjie, D. *Acc. Chem. Res.* **2002**, *35*, 1035−1044.
(19) Flahaut, E.; Peigney, A.; Laurent, Ch.; Rousset, A. *J. Mater. Chem.* **2000**, *10*, 249−252.
(20) Hou, H.; Schaper, A. K.; Jun, Z.; Weller, F.; Greiner, A. *Chem. Mater.* **2003**, *15*, 580−585.
(21) Cassell, A. M.; Raymakers, J. A.; Kong, J.; Dai, H. *J. Phys. Chem. B* **1999**, *103*, 6484−6492.
(22) Park, C.; Keane, M. A. *J. Colloid Interface Sci.* **2002**, *250*, 37−48.
(23) Hafner, J. H.; Bronikowski, M. J.; Azamian, B. R.; Nikolaev, P.; Rinzler, A. G.; Colbert, D. T.; Smith, K. A.; Smalley, R. E. *Chem. Phys. Lett.* **1998**, *296*, 195−202.
(24) Alvarez, W. E.; Pompeo, F.; Herrera, J. E.; Balzano, L.; Resasco, D. E. *Chem. Mater.* **2002**, *14*, 1853−1858.
(25) Wei, B. Q.; Zhang, Z. J.; Ajayan, P. M.; Ramanath, G. *Carbon* **2002**, *40*, 47−51.
(26) Zheng, F.; Liang, L.; Gao, Y.; Sukamto, J. H.; Aardahl, C. L. *Nano Lett.* **2002**, *2*, 729−732.
(27) Gournis, D.; Karakassides, M. A.; Bakas, T.; Boukos, N.; Patridis, D. *Carbon* **2002**, *40*, 2641−2646.
(28) Zhang, W. D.; Phang, I. Y.; Liu, T. X. *Adv. Mater.* **2006**, *18*, 73−77.
(29) Bakandritsos, A.; Simopoulos, A.; Petridis, D. *Nanotechnology* **2006**, *17*, 1112−1127.
(30) Nweman, A. C. D. *Mineralogical Society Monograph No. 6*; John Wiley & Sons: New York, 1987.
(31) Zhang, A.; Li, C.; Bao, S.; Xu, Q. *Microporous Mesoporous Mater.* **1999**, *29*, 383−388.
(32) Velasco-Santos, C.; Martýñez-Hernàndez, A. L.; Fisher, F. T.; Ruoff, R.; Castaño, V. M. *Chem. Mater.* **2003**, *15*, 4470−4475.
(33) Bourlinos, A. B.; Karakassides, M. A.; Simopoulos, A.; Petridis, D. *Chem. Mater.* **2000**, *12*, 2640−2645.
(34) Fonseca, A.; Hernadi, K.; Piedigrosso, P.; Colomer, J. F.; Mukhopadhyay, K.; Doome, R. *Appl. Phys. A: Mater. Sci. Process.* **1998**, *67*, 11−22.
(35) Fu, H. K.; Du, M.; Zheng, Q. *Appl. Surf. Sci.* **2011**, *257*, 8981−8984.
(36) Cheng, J. P.; Zhang, X. B. Doctor-Degree Dissertation, Zhejiang University, 2005.
(37) Li, Q. W.; Yan, H.; Ye, Y. C.; Zhang, J.; Liu, Z. F. *J. Phys. Chem. B* **2002**, *106*, 11085−11088.

(38) Ye, L.; Wu, J. H. Master-Degree Dissertation, Huaqiao University, 2005.

(39) Wang, J. F.; Du. B. Z. Master-Degree Dissertation, Xian University of Technology, 2006.

(40) Xu, D.; Zhou, X.; Wang, X. K. *Appl. Clay Sci.* **2008**, *39*, 133−141.

(41) Bhattacharyya, K. G.; Gupta, S. S. *Adv. Colloid Interfac.* **2008**, *140*, 114−131.

(42) Wang, H. X. *Bentonite* **1980**.

(43) Yuan, P.; Annabi-Bergaya, F.; Tao, Q.; Fan, M. D.; Liu, Z. W.; Zhu, J. X.; He, H. P.; Chen, T. H. *J. Colloid Interface Sci.* **2008**, *324*, 142−149.

(44) Wang, L. B.; Xiang, S. F.; Ten, Y. J.; Hua, T. W. *Acta Petrol. Sin.* **1989**, *5*, 46−53.